Editors' Suggestion

Oil-coated bubble formation from submerged coaxial orifices

Bingqiang Ji, Zhengyu Yang, and Jie Feng*
Department of Mechanical Science and Engineering, University of Illinois at Urbana–Champaign, Urbana, Illinois 61801, USA

(Received 29 November 2020; accepted 17 February 2021; published 17 March 2021)

Dispersions of bubbles with a compound interface in liquids are ubiquitous in nature and various industrial processes, such as marine oil transport and froth flotation, hence understanding surface phenomena effect on bubble formation in liquids remains as a canonical topic in fundamental multiphase flows. Here, we experimentally investigate the formation of an oil-coated bubble at submerged coaxial orifices in quiescent liquids. The air bubble is initially injected inside a confined oil domain and then exits into the surrounding water under buoyancy, forming an oil-coated bubble. Compared with the bubble formation in a single-phase liquid, the bubble size is significantly modified due to the presence of the oil phase. We develop a force balance model to predict the oil-coated bubble size, considering the orifice geometry as well as the compound air/oil/water interface, which agrees well with the experimental results. We further discuss the dependencies of the bubble size on the Bond number, size ratio of the coaxial orifices, and the interfacial tension ratio of oil-water and oil-air interfaces. Our study could contribute to further understandings on the dynamics of bubble formation with a compound interface.

DOI: 10.1103/PhysRevFluids.6.033602

I. INTRODUCTION

Dispersions of gas bubbles in liquids are widely present in natural phenomena and various industrial processes [1–3]. In typical scenarios, the bubble is coated by either particulate matters or bulk impurities, forming a "compound" gas-liquid interface. For instance, gas bubbles coated by oil layers were observed to be released from the continuous natural seeps in the deep sea [4], which act as important carriers for the transport of natural hydrocarbon and oil spill from deep sea to marine surface [5–7]. In addition, bubbles coated with an oily phase have been used to enhance the flotation performance of mineral separations [8] and oil recovery [9]. Bubbles with such a three-phase interface formed by phase change in heat exchangers also play a key role in the heat and mass transfer in power production, solar energy equipment, and water desalination [10,11]. In the above examples, the compound interface has been found to significantly modify and enrich the bubble dynamics [12,13] as well as raise the question of how to understand the role of a compound interface in various scenarios, such as the bubble formation.

For instance, the formation of bubbles in a multiphase liquid system is much less studied. Most of the literatures consider the gas bubble formation in a single-phase liquid [14]. In particular, Tate's law [15] is used to predict the size of a bubble quasistatically formed at an orifice in a quiescent liquid [16], which balances the buoyant force and capillary force and can be expressed as

$$\frac{d_g}{d_{ni}} = \left(\frac{\rho_w d_{ni}^2 g}{6\gamma_{wg}}\right)^{-1/3}, \tag{1}$$

*jiefeng@illinois.edu

where d_g is the bubble diameter, d_{ni} is the orifice diameter, ρ_w is the water density, γ_{wg} is the surface tension of water, and g is the gravitational acceleration. Although a wide variety of investigations have been carried out regarding the effects of fluid properties [17], orifice shape [18], orifice wettability [19], gas flow rate [20], and liquid height [21], very few of them consider the formation of bubbles with an oil coating. Only until recently, Wang *et al*. [22] studied the formation of oil-coated bubbles using an oil-filled chamber with an orifice at the top in a liquid pool. They found that Tate's law failed to predict the oil-coated bubble size, and they revised Tate's law by fitting their experimental results using an effective bubble/fluid interfacial tension defined as the sum of the oil/water and oil/gas interfacial tensions. Though coaxial orifices have been used widely to generate oil-coated bubbles [23,24] and compound droplets [25,26], to our best knowledge, quantification of how the orifice geometry and the compound interface influence the oil-coated bubble size remains to be an open question.

In this work, we study the quasistatic formation of an oil-coated bubble at coaxial orifices in the presence of a confined oil domain. A coaxial orifice system is developed to generate oil-coated bubbles, where the coaxial orifice geometry and the oil-water interfacial tension are systematically changed to quantify their influences on the bubble size. A theoretical model based on the quasistatic force balance is developed to predict the bubble size. This model is verified by comparing with the experimental results, and the effects of the dimensionless numbers are further discussed with force analysis.

II. EXPERIMENTS

The schematic of the experimental system is shown in Fig. 1(a). A coaxial orifice system was designed by plugging a metal needle into a Teflon pipe with a rubber plug, where the inner needle was located at the center of the outer pipe with the needle above the pipe exit. The coaxial orifice system was placed at the bottom of a square transparent acrylic plastic tank filled with water, with a cross-section of 40×40 mm^2 and a height of 60 mm. The dimensions of the tank were much larger than the bubble size to minimize the effects of the walls and the water meniscus. A sessile oil droplet was formed above the pipe initially by injecting the oil through the outer pipe using a syringe pump (11 Pico Plus Elite, Harvard Apparatus) to control the oil volume. Next, the air was injected through the inner needle using another syringe pump (PHD ULTRA, Harvard Apparatus) to generate the oil-coated bubble. The flow rates of the oil and gas were controlled to be 5–30 μl/min. Such small flow rates were chosen to ensure a quasistatic formation process and negligible viscous effects on the bubble size, as confirmed by Fig. 2. The images were captured by a high-speed camera (FASTCAM Mini AX200, Photron) with a frame rate of 2000 frames per second, an exposure time of 250 or 500 μs, and a resolution of 1024×1024 pixels. A lens system ($12\times$ zoom lens system, Navitar) with a magnification of 1.5–3.0 was used for obtaining close-up views of the bubble illuminated by a LED panel. The snapshot just after the oil-coated bubble pinch-off [as shown in Fig. 1(c)] was chosen to extract the boundaries between different phases. The volumes of the gas phase (V_g) and oil phase (V_o) of the formed oil-coated bubble were calculated by image analysis. Then, the equivalent diameter of the oil-coated bubble, $d_g = (6V_g/\pi)^{1/3}$, as well as the oil fraction of the oil-coated bubble, $f_o = V_o/(V_g + V_o)$, can be quantified. The physical properties of deionized (DI) water and silicone oils are listed in Table I, where the surface tensions of the liquids and their interfacial tensions were measured using the pendant-drop method.

The schematic of the oil-coated bubble formation is shown in Fig. 1(b). Since the silicone oil always wets the pipe and needle, the oil-water-solid and the oil-gas-solid contact lines are pinned at the outer edge of the pipe and the inner edge of the needle. Therefore, the formation process is expected to be controlled by the outer diameter of the pipe and the inner diameter of the needle, d_{po} and d_{ni}, respectively. The height of the needle above the pipe is denoted as h_{pn}, and the sessile oil droplet has an initial height of h_{po} [see Fig. 1(c)]. The typical features of the oil-coated bubble formation process with 10 cSt silicone oil in DI water are shown in Fig. 1(c), where $d_{po} = 4.76$ mm, $d_{ni} = 0.84$ mm, $h_{pn} = 0.75$ mm, and $h_{po} = 1.43$ mm. An air bubble is first

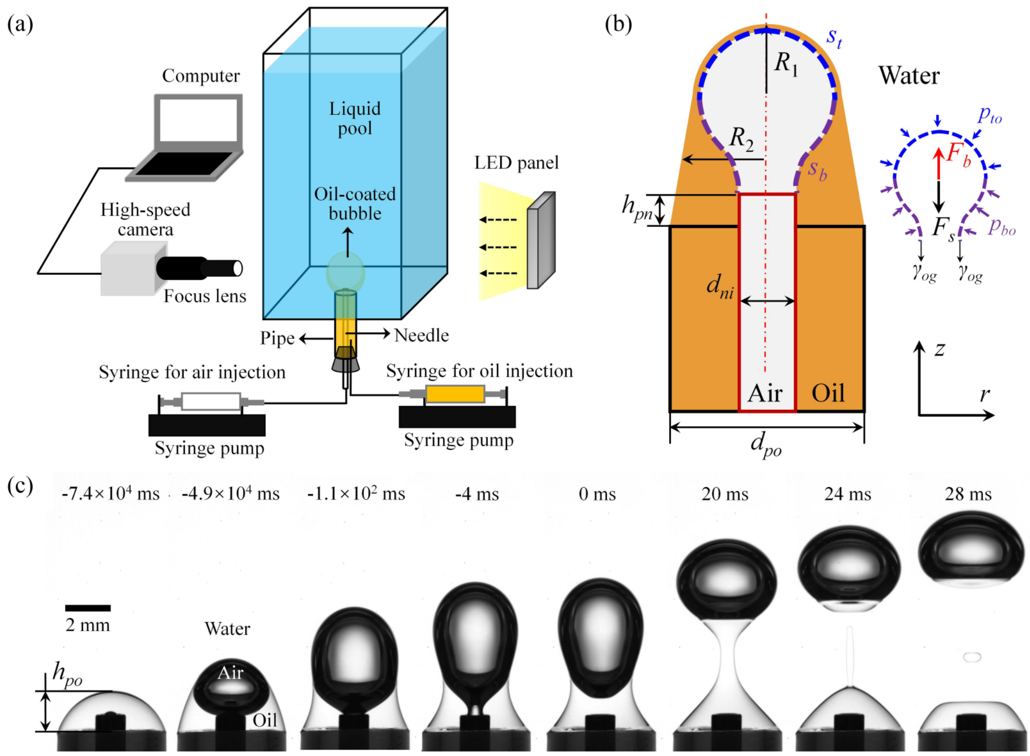

FIG. 1. The experimental configuration and snapshots of oil-coated bubble formation. (a) Schematic of the experimental apparatus. The oil-coated bubble is generated from a coaxial system consisting of a pipe and a needle. The oil and gas are injected using two syringe pumps through the pipe and the needle, respectively. (b) Schematic of the oil-coated bubble formation when the gas neck forms. The inset shows a free-body diagram for the quasistatic force model. The white, orange and grey represent the water, oil and gas phases, respectively. (c) Experimental snapshots of the oil-coated bubble formation with 10 cSt silicone oil in DI water, where the moment at the pinch-off of the air bubble neck is denoted as $t = 0$. An oil droplet pinned at the pipe edge was formed first and then the air was injected. An oil-coated bubble was formed with an equivalent diameter of 4.33 mm and an oil fraction of 0.10. Here, $d_{po} = 4.76$ mm, $d_{ni} = 0.84$ mm, $h_{pn} = 0.75$ mm, and $h_{po} = 1.43$ mm.

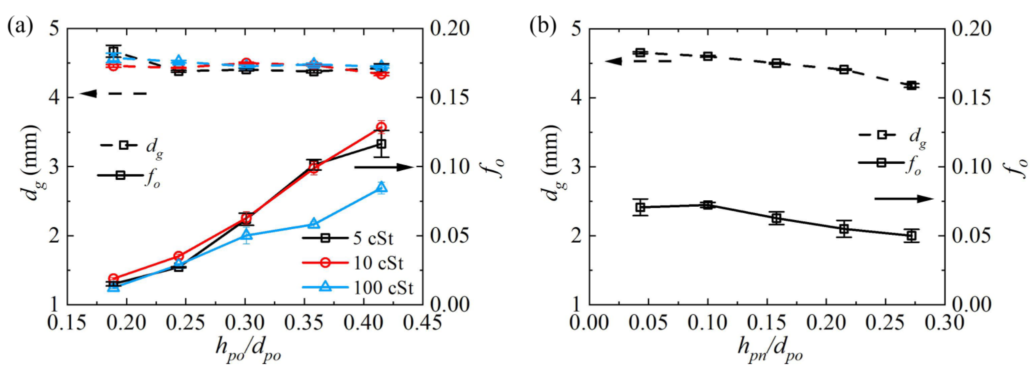

FIG. 2. Dependencies of the equivalent diameter d_b and oil fraction f_o of the oil-coated bubble on (a) the oil drop height h_{po} with $h_{pn} = 0.16d_{po}$ and different oil viscosities, and (b) the height of needle above the pipe h_{pn} with $h_{po} = 0.30d_{po}$ and 10 cSt silicone oil. $d_{po} = 6.35$ mm and $d_{ni} = 2.11$ mm in all cases.

TABLE I. Physical properties of the liquids used in the experiments (g: gas; o: oil; w: water).

Liquids	ρ (kg/m^3)	μ (mPa s)	γ_{wg} (mN/m)	γ_{ow} (mN/m)	γ_{og} (mN/m)
DI water	998	0.89	71.6 ± 1.0	N/A	N/A
5 cSt silicone oil	913	4.6	N/A	38.1 ± 0.4	18.7 ± 0.3
10 cSt silicone oil	930	9.3	N/A	40.9 ± 0.5	19.1 ± 0.3
100 cSt silicone oil	960	96	N/A	43.7 ± 0.4	20.1 ± 0.2

generated from the needle inside the sessile oil droplet, and it grows with its top coated by an oil film. Then a gas neck formed at the bottom of the air bubble and pinches off rapidly (−4–0 ms). The bubble rises under buoyancy, and stretches the oil below it into an oil column (0–20 ms). After the oil column pinches off, an oil-coated bubble is formed with $d_g = 4.18$ mm and $f_o = 0.10$ (24–28 ms). Considering γ_{wg}–$(\gamma_{og} + \gamma_{ow}) > 0$ (see Table I), the silicone oils spontaneously spread on the water-air interface and completely coat the bubble in the current study. No oil film rupture or retraction on the bubble surface is observed during the whole formation process, and the oil-coated bubble finally rises with an oil tail at the bottom. We note that the pinch-off of the gas neck determines the bubble size while the following pinch-off of the oil column sets the oil fraction.

The dependencies of d_g and f_o on the oil viscosity (μ_o), h_{pn}, and h_{po} are experimentally investigated, as shown in Fig. 2. In the current experimental regime, f_o increases with μ_o and h_{po} while unaffected by h_{pn}, and $f_o < 0.13$ in all cases. On the other hand, μ_o, h_{pn} and h_{po} are found to have negligible effects on d_g, suggesting that the formation of the oil-coated bubble is quasistatic and could be estimated by the balance between buoyant and capillary forces. Therefore, in the followings, we will first establish a theoretical model for the bubble size based on force balance. Then the model will be validated by comparison with the experimental results using different d_{po} and d_{ni} as well as γ_{ow}. 10 cSt silicone oil is used with $h_{pn} = 0.16 d_{po}$ and $h_{po} = 0.30 d_{po}$ in the following experiments, and γ_{ow} is changed by using aqueous solutions of sodium dodecyl sulfate (SDS, BioXtra, ⩾99% (GC), Sigma-Aldrich) with a mass concentration of 0.01%–1%, as shown in Table II.

III. THEORETICAL MODELING

Here we use the static force balance at the moment when the gas neck appears to solve for the equivalent bubble diameter d_g, as depicted by Fig. 1(b). The oil fully coats the bubble as shown in Fig. 1(c) due to the complete wetting state. Assuming that the formation process is axisymmetric, the air bubble suffers from a downward surface tension force F_s exerted by the needle and an upward force F_b coming from the static pressure of the surrounding liquids. Here we specify that a positive force has an upward direction. At the instant when the gas neck appears, we have

$$F_s + F_b = 0, \tag{2}$$

where

$$F_s = -\pi d_{ni} \gamma_{og} \tag{3}$$

and $F_b = \mid \int_s p d\boldsymbol{A} \mid$ with p denoted as the hydrostatic pressure at the air bubble surface, as shown in Fig. 1(b).

TABLE II. Interfacial tensions of different aqueous SDS solutions with 10 cSt silicone oil.

SDS mass concentration (%)	0.01	0.05	0.1	0.2	1
γ_{ow} (mN/m)	36.0 ± 0.8	30.3 ± 1.3	22.5 ± 0.4	14.2 ± 0.3	10.9 ± 0.1

To model F_b, the shape for the oil-water interface is approximated as the peripheral surface of a truncated circular cone with a base diameter of d_{po}, connected with a hemispheric surface with a radius of R_1. Therefore, F_b can be written as

$$F_b = \int_{s_b} p_{bo} dA_r - \int_{s_t} p_{to} dA_r, \tag{4}$$

where s_b and s_t represent the oil/gas interfaces of the bottom cone and the top hemisphere, respectively. A_r is the projected area of the bubble surface of interest on the horizontal plane. p_{to} and p_{bo} represent the pressures of the surrounding oils in the top oil film and the bottom oil domain, respectively. We obtain

$$p_{bo} = p_{bw} + \frac{\gamma_{ow}}{R_2}, \quad p_{to} = p_{tw} + \frac{2\gamma_{ow}}{R_1}, \tag{5}$$

where p_{tw} and p_{bw} are the hydrostatic pressures of the water at the same level with the bubble surface of interest, respectively, while R_2 is the radius of curvature of the peripheral surface of the truncated cone. Now, Eq. (4) can be expressed as

$$F_b = \left(\int_{s_t} p_{bw} dA_r - \int_{s_b} p_{tw} dA_r\right) + \left(\int_{s_t} \frac{\gamma_{ow}}{R_2} dA_r - \int_{s_b} \frac{2\gamma_{ow}}{R_1} dA_r\right) = F_{b1} + F_{b2}. \tag{6}$$

We calculate F_{b1} using the buoyant force suffered by an air bubble with a diameter of d_g in water, i.e.,

$$F_{b1} = \rho_w \frac{\pi}{6} d_g^3 g. \tag{7}$$

According to Fig. 1(b), we further approximate that $R_1 = d_g/2$, and R_2 equals the average radius of curvature of the peripheral surface of the truncated cone, $(d_g + d_{po})/4$, and then we have

$$F_{b_2} = \left(\frac{\gamma_{ow}}{R_2} - \frac{2\gamma_{ow}}{R_1}\right)\pi R_1^2 = -\pi \frac{d_g d_{po}}{d_g + d_{po}} \gamma_{ow}, \tag{8}$$

which can be interpreted as a capillary force originating from the distinct oil layer geometries above and below the inner air bubble, contributing to the static force at the oil/gas interface.

If we balance F_{b1} with F_s, we obtain Tate's law from Eq. (2), as shown in Eq. (1). Substituting Eq. (3) and Eqs. (6)– (8) into Eq. (2) and defining the dimensionless numbers of

$$D_g = \frac{d_g}{d_{ni}}, \quad A_d = \frac{d_{po}}{d_{ni}}, \quad A_\gamma = \frac{\gamma_{ow}}{\gamma_{og}}, \tag{9}$$

which represent the dimensionless equivalent bubble diameter, the coaxial orifice size ratio, and the interfacial tension ratio, respectively, we obtain the dimensionless form of Eq. (2) as

$$\frac{1}{6}\mathrm{Bo} D_g^3 - A_\gamma \frac{A_d D_g}{A_d + D_g} - 1 = 0, \tag{10}$$

where $\mathrm{Bo} = \rho_w d_{ni}^2 g/\gamma_{og}$, as a revised Bond number which compares gravitational force with the surface tension force. The size of the oil-coated bubble formed at coaxial orifices can be calculated analytically by solving Eq. (10), which is only determined by three dimensionless numbers of Bo, A_γ, and A_d. In the next section, this model will be validated with experimental results first and then adopted to discuss the effects of the three dimensionless parameters on the bubble size.

IV. DISCUSSION

A. Model validation with the oil-coated bubble size

We experimentally investigated the dependence of the equivalent diameter of the oil-coated bubble generated in DI water, d_g, on the inner diameter of the needle, d_{ni}, when using different

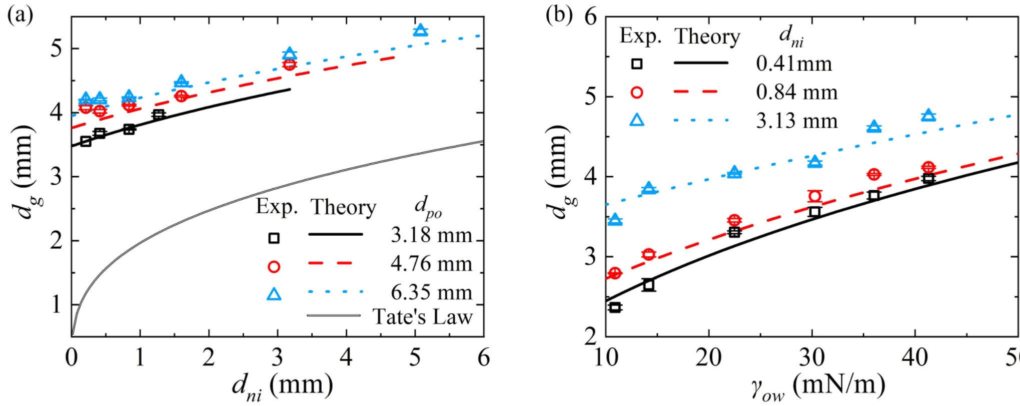

FIG. 3. Dependence of d_g on (*a*) the inner diameter of the needle d_{ni} with $d_{po} = 3.18$, 4.76, and 6.35 mm in DI water, and (*b*) the oil/water interfacial tension γ_{ow} with $d_{po} = 4.76$ mm and $d_{ni} = 0.41$, 0.84, and 3.18 mm. 10 cSt silicone oil and aqueous SDS solutions are used. The hollow points and lines represent the experimental and theoretical [Eq. (10)] results, respectively.

d_{po}, as shown in Fig. 3(a). Regarding the effect of the orifice geometry, d_g increases with d_{ni}, due to a large surface tension force F_s exerted on the bubble. Meanwhile, increasing d_{po} enlarges the downward F_{b2} [see Eq. (8)], which needs to be offset by larger upward F_{b1}, resulting in larger d_g. In addition, Fig. 3(b) shows the dependencies of d_g on γ_{ow} with different SDS solutions and inner needles. Smaller γ_{ow} reduces the Laplace pressure caused by the oil-water interface, which corresponds to smaller downward F_{b2}, for smaller d_g.

For comparison, the theoretical values of d_g calculated by Eq. (10) are plotted in Fig. 3, showing that our theoretical model quantitatively predicts the experimental results well, validating the accuracy of this model. Figure 3(a) also shows the results of the size of the air bubble calculated with Tate's law, i.e., the size of the bubble generated from the same needle in water without the presence of oil. Comparing our model with Tate's law, it can be found that the presence of the confined oil domain around the air bubble significantly increases the formed bubble size since the compound interface modifies the capillary force. We will further discuss the effects of the oil domain by dimensionless analysis in a large parameter space in next section.

B. Dimensionless analysis

In this section, the effects of Bo, A_d, and A_γ on D_g will be discussed based on our model. The available data from the literature will also be used to compare with our model. The theoretical predictions of D_g with Bo when $A_\gamma = 2.2$ and $A_d = 1$, 10, and 100 are shown in Fig. 4(a). It can be found that D_g decreases with Bo, showing an overall linear trend with a power law of $-1/3$ to $-1/2$ in a log-log plot. On the other hand, Tate's law gives a power-law relationship of $D_g = (\text{Bo}_w/6)^{-1/3}$ where $\text{Bo}_w = \rho_w d_{ni}^2 g/\gamma_{wg}$. Thus, changing the size of the confined oil domain modifies the power law of D_g with Bo because of the role of the capillary force coming from the oil/water interface.

Now, we focus on explaining the variation of the power law between D_g and Bo based on force analysis. The comparisons of F_{b1} and F_{b2} with F_s can be expressed as

$$\frac{F_{b1}}{F_s} = -\frac{1}{6}\text{Bo}D_g^3, \quad \frac{F_{b2}}{F_s} = A_\gamma \frac{A_d D_g}{A_d + D_g}, \tag{11}$$

and their dependencies on Bo with $A_\gamma = 2.2$ and $A_d = 1$, 10, and 100 are given in Fig. 4(b). It shows that F_{b1} and F_{b2} are comparable, which means that the confined oil domain always plays an important role when $A_\gamma \sim 1$. When $A_d \gg 1$ and $\text{Bo} < 1$, F_s becomes negligible compared to F_{b1} and F_{b2}, thus the capillary force F_{b2} caused by the confined oil domain becomes the dominant force

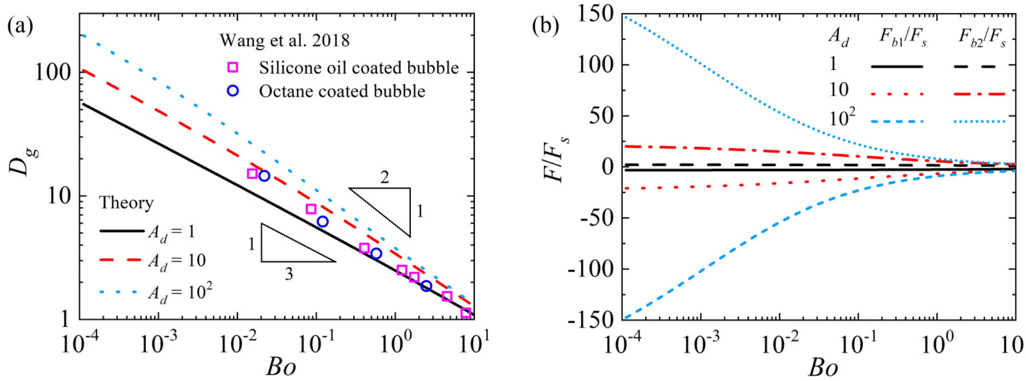

FIG. 4. Effect of Bo on the oil-coated bubble formation with $A_\gamma = 2.2$ and $A_d = 1$, 10, and 100: (a) the dimensionless equivalent bubble diameter D_g calculated by our theory [Eq. (10)], compared with the experiments of Wang *et al.* [22], and (b) dimensionless forces of F_{b1}/F_s and F_{b2}/F_s calculated theoretically.

of the oil-coated bubble formation, and the surface tension force from the oil-gas-needle triple line exerts negligible effect, resulting in the oil-coated bubble size far from the prediction by Tate's law [as shown in Fig. 3(a)]. Neglecting F_s and using $A_d \gg 1$ in Eq. (10), we can find the upper limit of D_g as

$$D_g \sim \left(\frac{\mathrm{Bo}}{6A_\gamma}\right)^{-1/2} = \left(\frac{\rho_w d_{ni}^2 g}{6\gamma_{ow}}\right)^{-1/2}, \tag{12}$$

giving a power law of $-1/2$ followed by the results with larger A_d in Fig. 4(a). When $A_d \sim 1$, considering that $D_g \gg 1$ with $\mathrm{Bo} < 1$, the lower limit of D_g can be obtained from Eq. (10) as

$$D_g \sim \left(\frac{\mathrm{Bo}}{6(A_\gamma + 1)}\right)^{-1/3} = \left(\frac{\rho_w d_{ni}^2 g}{6(\gamma_{ow} + \gamma_{og})}\right)^{-1/3}, \tag{13}$$

which gives a power law of $-1/3$ followed by the results with smaller A_d in Fig. 4(a). It shows that when $d_{po} \approx d_{ni}$, the sessile oil drop becomes a thin oil film around the air bubble at the detaching moment, thus the bubble size can be predicted by Tate's law using an effective interfacial tension of $\gamma_{ow} + \gamma_{og}$ for such an air/oil/water interface.

We also compare our model prediction with the available data from Wang *et al.* [22], as shown in Fig. 4(a). They fitted their experimental D_g as a function of a revised Bond number (based on the effective interfacial tension of $\gamma_{ow} + \gamma_{og}$), and found a power law of -0.41. Their experimental results are plotted in Fig. 4(a) which are located in the region between $A_d \approx 1 - 10$ with $\mathrm{Bo} \approx 10^{-2}$–10. In Wang *et al.* [22], the oil domain size was not confined. Considering the complete wetting state between the oil and chamber, we estimate their oil domain size d_{po} using the capillary length l_c below which the surface tension dominates [27], i.e., $d_{po} \approx l_c = [\gamma_{ow}/(\rho_w - \rho_o)g]^{1/2}$, which means that $A_d \approx O(1) - O(10)$ with Bo $[=d_{ni}^2/(\gamma_{og}/\rho_w g)]$ $\approx O(1) - O(10^{-2})$ in their experiments. Thus, considering the power law between D_g and Bo, the experimental data should follow $-1/3$ when $A_d \approx 1$ and $\mathrm{Bo} \approx O(1)$, while the trend is expected to change to $-1/2$ for $A_d \approx 10$ and $\mathrm{Bo} \approx O(10^{-2})$. As shown in Fig. 4, the power law by fitting their experimental data is -0.41, between $-1/3$ and $-1/2$, consistent with the model prediction. We believe this not only validates our theoretical model, but also illustrates that our model can accurately quantify the influence of the confined oil domain by considering the coaxial orifice size ratio and the interfacial tension ratio.

The effects of A_d (when $\mathrm{Bo} = 10^{-2}$) and A_γ (when $A_d = 10$) on D_g, are further shown in Fig. 5, with the corresponding forces. Increasing A_d enlarges D_g by increasing F_{b2}/F_s, as shown in Eq. (11) and Figs. 5(a) and 5(b). In particular, the bubble size increasing effect of A_d is more significant for

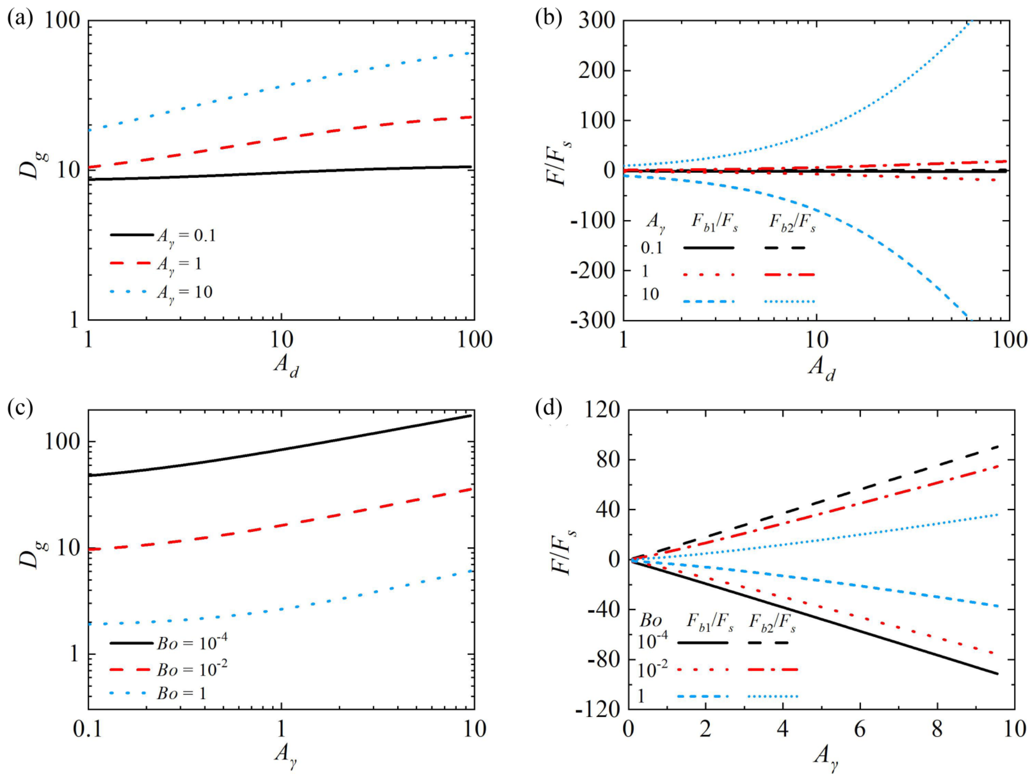

FIG. 5. Dependencies of dimensionless equivalent bubble diameter, D_g, and the dimensionless forces, F_{b1}/F_s and F_{b2}/F_s, on (a), (b) A_d with Bo $= 10^{-2}$ and $A_\gamma = 0.1$, 1, and 10 and (c), (d) A_γ with $A_d = 10$ and Bo $= 10^{-4}$, 10^{-2}, and 1.

larger A_γ. In fact, it can be found that when $A_\gamma < 1$, i.e., $\gamma_{ow} < \gamma_{og}$, F_s should be considered even with large A_d and small Bo. In addition, D_g increases with A_γ because F_{b2}/F_s increases linearly with A_γ, as shown in Eq. (11) and Figs. 5(c) and 5(d), making the evolution of D_g with A_γ at different Bo show the same trend. Therefore, the size of oil-coated bubbles can be controlled quantitatively by adjusting the coaxial orifice size ratio and the interfacial tension ratio.

V. CONCLUSION

In this work, we investigate the formation of oil-coated bubbles at submerged coaxial orifices in the presence of a confined oil domain in quiescent liquids experimentally and theoretically. The air bubble was generated from an inner orifice inside an oil domain confined by an outer orifice, and then exited into the water under buoyancy. We document that the presence of oil significantly increases the bubble size, compared with the case in water. We develop a theoretical model with force balance to predict the size of the oil-coated bubbles, considering the orifice geometry as well as the compound air-oil-water interface. Based on Tate's law, this model introduces a force originating from the Laplace pressure difference caused by the distinct oil layer geometries at the top and bottom of the bubble. The model is further validated with our experimental results as well as the available data in the literature. The oil-coated bubble size is controlled by three dimensionless numbers, which are Bond number, coaxial orifice size ratio, and interfacial tension ratio of oil-water and oil-air interfaces. We show that the power law between the dimensionless bubble size and Bond number changes from $-1/3$ to $-1/2$ when the coaxial orifice size ratio increases, and we quantify the dependencies of the bubble size on the coaxial orifice ratio and interfacial tension ratio, which is explained further based on force analysis. Overall, our study could exemplify the role of the compound interface for the oil-coated bubble formation in a multiphase fluid system, which contributes to further understandings for bubble dynamics with a compound interface. Our work may also offer modeling insights in determining the size of the compound droplets from coaxial orifices [25,26] with further consideration required to include the flow contribution, such as inertial and viscous forces for a wide range of parameters [14,28,29]. The results may be useful in estimating the size distribution of oil-coated bubbles as an input to the characterization of the transport and dynamics of bubbly flows in natural and industrial processes where compound interfaces are present.

In addition, the dynamical aspects of the compound bubble formation remain to be explored, such as the dependence of the oil-coated bubble size on the flow rate, and the sequential pinch-off dynamics of the gas neck and oil column determining the oil fraction of the compound bubble. After being released, the oil-coated bubble rises under buoyancy and interacts with the surrounding liquids, and the oil coating may play an important role for the bubble dynamics, which will also be the focus of our future work.

ACKNOWLEDGMENTS

This work is partially supported by American Chemical Society Petroleum Research Fund Grant No. 61574-DNI9 (to J.F.).

---

[1] S. Takagi and Y. Matsumoto, Surfactant effects on bubble motion and bubbly flows, Annu. Rev. Fluid Mech. **43**, 615 (2011).

[2] F. Risso, Agitation, mixing, and transfers induced by bubbles, Annu. Rev. Fluid Mech. **50**, 25 (2018).

[3] Y. Zhou, C. Zhao, and H. Bo, Analyses and modified models for bubble shape and drag coefficient covering a wide range of working conditions, Int. J. Multiphase Flow **127**, 103265 (2020).

[4] C. Johansen, A. C. Todd, and I. R. MacDonald, Time series video analysis of bubble release processes at natural hydrocarbon seeps in the northern gulf of mexico, Mar. Petrol. Geol. **82**, 21 (2017).

[5] F. S. Ehrenhauser, P. Avij, X. Shu, V. Dugas, I. Woodson, T. Liyana-Arachchi, Z. Zhang, F. R. Hung, and K. T. Valsaraj, Bubble bursting as an aerosol generation mechanism during an oil spill in the deep-sea environment: Laboratory experimental demonstration of the transport pathway, Environ. Sci-Proc. Imp. **16**, 65 (2014).

[6] J. Feng, M. Roché, D. Vigolo, L. N. Arnaudov, S. D. Stoyanov, T. D. Gurkov, G. G. Tsutsumanova, and H. A. Stone, Nanoemulsions obtained via bubble-bursting at a compound interface, Nat. Phys. **10**, 606 (2014).

[7] P. S. Stewart, J. Feng, L. S. Kimpton, I. M. Griffiths, and H. A. Stone, Stability of a bi-layer free film: Simultaneous or individual rupture events? J. Fluid Mech. **777**, 27 (2015).

[8] F. Zhou, L. Wang, Z. Xu, Q. Liu, M. Deng, and R. Chi, Application of reactive oily bubbles to bastnaesite flotation, Miner. Eng. **64**, 139 (2014).

[9] L. Su, Z. Xu, and J. Masliyah, Role of oily bubbles in enhancing bitumen flotation, Miner. Eng. **19**, 641 (2006).

[10] T. S. Emery, P. A. Raghupathi, and S. G. Kandlikar, Bubble growth inside an evaporating liquid droplet introduced in an immiscible superheated liquid, Int. J. Heat Mass Tran. **127**, 313 (2018).

[11] S. S. Sadhal, P. S. Ayyaswamy, and J. N. Chung, *Transport Phenomena with Drops and Bubbles* (Springer Science & Business Media, New York, 2012).

[12] S. Mandal, U. Ghosh, and S. Chakraborty, Effect of surfactant on motion and deformation of compound droplets in arbitrary unbounded stokes flows, J. Fluid Mech. **803**, 200 (2016).

[13] J. Magnaudet and M. J. Mercier, Particles, drops, and bubbles moving across sharp interfaces and stratified layers, Annu. Rev. Fluid Mech. **52**, 61 (2020).

[14] A. A. Kulkarni and J. B. Joshi, Bubble formation and bubble rise velocity in gas-liquid systems: A review, Ind. Eng. Chem. Res. **44**, 5873 (2005).

[15] T. Tate, Xxx. on the magnitude of a drop of liquid formed under different circumstances, Lond. Edinb. Dubl. Phil. Mag. **27**, 176 (1864).

[16] J. Feng, M. Muradoglu, H. Kim, J. T. Ault, and H. A. Stone, Dynamics of a bubble bouncing at a liquid/liquid/gas interface, J. Fluid Mech. **807**, 324 (2016).

[17] W. Abbassi, S. Besbes, M. El Hajem, H. B. Aissia, J. Champagne, and J. Jay, Influence of operating conditions and liquid phase viscosity with volume of fluid method on bubble formation process, Eur. J. Mech. B-Fluid **65**, 284 (2017).

[18] P. Hanafizadeh, A. Sattari, S. E. Hosseini-Doost, A. G. Nouri, and M. Ashjaee, Effect of orifice shape on bubble formation mechanism, Meccanica **53**, 2461 (2018).

[19] S. Gnyloskurenko, A. Byakova, O. Raychenko, and T. Nakamura, Influence of wetting conditions on bubble formation at orifice in an inviscid liquid. transformation of bubble shape and size, Colloids Surf. A **218**, 73 (2003).

[20] H. Xiao, S. Geng, A. Chen, C. Yang, F. Gao, T. He, and Q. Huang, Bubble formation in continuous liquid phase under industrial jetting conditions, Chem. Eng. Sci. **200**, 214 (2019).

[21] Y. Zhou, B. Ji, C. Zhao, and H. Bo, Bubble formation from a submerged orifice in a thin liquid layer: Detachment and bursting, Phys. Fluids **33**, 013305 (2021).

[22] S. Wang, Y. Zhang, J. C. Meredith, S. H. Behrens, M. K. Tripathi, and K. C. Sahu, The dynamics of rising oil-coated bubbles: Experiments and simulations, Soft Matter **14**, 2724 (2018).

[23] Y. H. Mori, Configurations of gas-liquid two-phase bubbles in immiscible liquid media, Int. J. Multiphase Flow **4**, 383 (1978).

[24] J. Xu, R. Chen, Y. Wang, and G. Luo, Controllable gas/liquid/liquid double emulsions in a dual-coaxial microfluidic device, Lab Chip **12**, 2029 (2012).

[25] N. Blanken, M. S. Saleem, C. Antonini, and M. Thoraval, Rebound of self-lubricating compound drops, Sci. Adv. **6**, eaay3499 (2020).

[26] N. Blanken, M. S. Saleem, M. Thoraval, and C. Antonini, Impact of compound drops: A perspective, Curr. Opin. Colloid Interf. Sci. **51**, 101389 (2020).

[27] P. De Gennes, F. Brochard-Wyart, and D. Quéré, *Capillarity and Wetting Phenomena: Drops, Bubbles, Pearls, Waves* (Springer Science & Business Media, New York, 2013).

[28] M. Jamialahmadi, M. R. Zehtaban, H. Müller-Steinhagen, A. Sarrafi, and J. M. Smith, Study of bubble formation under constant flow conditions, Chem. Eng. Res. Des. **79**, 523 (2001).

[29] J. Ma, J. Li, P. Zhou, Y. Song, L. Chai, and C. Q. Zhou, A viewpoint on the dynamics of bubble formation from a submerged nozzle, Eur. J. Mech. B-Fluid **78**, 276 (2019).